A Thermodynamic Investigation of Ni on Thin-Film Titanates (ATiO$_3$)

Chao Lin [1], Alexandre C. Foucher [2], Eric A. Stach [2] and Raymond J. Gorte [1,*]

[1] Department of Chemical and Biomolecular Engineering, University of Pennsylvania, 34th Street, Philadelphia, PA 19104, USA; linchao@seas.upenn.edu

[2] Department of Materials Science and Engineering, University of Pennsylvania, Philadelphia, PA 19104, USA; afoucher@seas.upenn.edu (A.C.F.); stach@seas.upenn.edu (E.A.S.)

[*] Correspondence: gorte@seas.upenn.edu

check for
updates

Abstract: Thin, ~1-nm films of CaTiO$_3$, SrTiO$_3$, and BaTiO$_3$ were deposited onto MgAl$_2$O$_4$ by Atomic Layer Deposition (ALD) and then studied as catalyst supports for ~5 wt % of Ni that was added to the perovskite thin films by Atomic Layer Deposition. Scanning Transmission Electron Microscopy demonstrated that both the Ni and the perovskites uniformly covered the surface of the support following oxidation at 1073 K, even after redox cycling, but large Ni particles formed following a reduction at 1073 K. When compared to Ni/MgAl$_2$O$_4$, the perovskite-containing catalysts required significantly higher temperatures for Ni reduction. Equilibrium constants for Ni oxidation, as determined from Coulometric Titration, indicated that the oxidation of Ni shifted to lower P_{O_2} on the perovskite-containing materials. Based on Ni equilibrium constants, Ni interactions are strongest with CaTiO$_3$, followed by SrTiO$_3$ and BaTiO$_3$. The shift in the equilibrium constant was shown to cause reversible deactivation of the Ni/CaTiO$_3$/MgAl$_2$O$_4$ catalyst for CO$_2$ reforming of CH$_4$ at high CO$_2$ pressures, due to the oxidation of the Ni.

Keywords: Atomic Layer Deposition; Ni catalyst; reforming catalyst; thermodynamics

1. Introduction

Perovskite-supported catalysts have received a great deal of attention recently because they offer the possibility of redispersing the metal if the crystallites become large due to sintering. Redispersion in these so-call "intelligent" catalysts occurs when the metal cations become part of the bulk lattice under oxidizing conditions, and then ex-solve back to the surface upon high-temperature reduction [1–8]. Originally proposed for use in automotive-emission-control catalysis, the idea has also shown promise for Solid Oxide Fuel Cell (SOFC) anodes [9,10] and steam-reforming catalysts [11–13], due, in part, to the improved thermal stabilities, but also due to improved tolerance against coking [14,15].

The application of perovskite supports has been limited due to the low specific surface areas of the perovskites, the sluggish kinetics for ingress and egress of metal particles, and the fact that some ex-solved metal remains embedded in the bulk, as discussed in more detail elsewhere [16]. Our group has prepared thin films of different perovskites on high-surface-area MgAl$_2$O$_4$ using Atomic Layer Deposition (ALD) in order to circumvent these limitations. For the materials to maintain a high surface area, the film thickness is limited to approximately 1 nm. This is demonstrated by the fact that a 1-nm film of SrTiO$_3$ on a 200-m^2/g support would have 0.96 g SrTiO$_3$/g of support, which results in a significantly lower specific surface area due to both the increased sample mass and decreased pore sizes of the sample. Although metals that are supported on these thin-film supports are not catalytically identical to bulk, ex-solution metals [17], many of their properties are similar. For example, most of these catalysts are only active after high-temperature reduction [18]. Perovskite-supported,

Ni catalysts also exhibit a high tolerance against coking [19,20]. Finally, supported Pt catalysts that are based on both thin-film and bulk perovskites showed similar differences from conventional Pt catalysts in their relative inactivity for hydrogenation reactions when compared to oxidation reactions [18].

There are indications that some of the support effects that are associated with perovskites are due to the formation of chemical bonds with the metal. First, the nature of interactions is metal and perovskite specific, as expected when chemical bonding is important. While Pt and Rh can enter the bulk $CaTiO_3$ lattice and both metals exhibit strong support interactions in their thin-film variants, Pd cannot be doped into $CaTiO_3$, and Pd supported on $CaTiO_3$ films shows normal behavior [17,18]. Metal-perovskite interactions were also shown to depend on the perovskite composition in a comparison of Rh catalysts that are supported on thin films of $CaTiO_3$, $SrTiO_3$, and $BaTiO_3$ [17]. Rh interacted very strongly with $CaTiO_3$, but only weakly with $BaTiO_3$. A second piece of evidence for bonding interactions is that the perovskite support can change the thermodynamic properties for oxidation of the supported metal. This was demonstrated for Ni on $LaFeO_3$ films, where the equilibrium constant for the reaction Ni to NiO was observed to shift by four orders of magnitude to lower PO_2 in the presence of the perovskite [20].

A better understanding of the nature of metal-perovskite interactions is clearly required before these materials can find wider application. In the present study, the equilibrium properties for Ni oxidation were examined on thin films of $CaTiO_3$, $SrTiO_3$, and $BaTiO_3$ that were supported on $MgAl_2O_4$. Ni-based catalysts are convenient for this comparison, because previous work has shown that the support can change the equilibrium constant for Ni oxidation to NiO by a significant amount. For the reaction, $Ni + O_2 = NiO$, the equilibrium constant, K_{NiO}, is equal to $P_{O_2}^-$ and is given by exp (-ΔG/RT), where ΔG is the free energy of reaction. K_{NiO}, and therefore ΔG, can be obtained by measuring the P_{O_2} at which both Ni and NiO exist in equilibrium. We will show that, similar to what was observed for Rh on these perovskite supports, Ni interacts most strongly with $CaTiO_3$, followed by $SrTiO_3$ and $BaTiO_3$.

2. Results

Table 1 provides a list of the samples that were used in this study, together with some of their key properties. The $CaTiO_3/MgAl_2O_4$, $SrTiO_3/MgAl_2O_4$, and $BaTiO_3/MgAl_2O_4$ supports were prepared while using procedures that are identical to those used in an earlier study of the support effects on Rh [17]. As in that case, the targeted perovskite film thicknesses were 1 nm, assuming that the perovskite film densities were the same as that of the corresponding bulk perovskites and that the 120-m^2/g $MgAl_2O_4$ was uniformly covered. The Ni loadings were achieved using five ALD cycles of the Ni precursor. The properties that are shown in the Table were measured after the sample had been oxidized and reduced five times at 1073 K in order to ensure that the samples had reached an equilibrium state.

Table 1. Key properties of the samples used in the study.

	Specific Surface Area (m^2/g) after 5 Redox Cycles at 1073 K	ALD Thin Film Loading (wt %)	Ni Loading (wt %)
Ni/MgAl$_2$O$_4$	115	N/A	4.8
Ni/CaTiO$_3$/MgAl$_2$O$_4$	73	29	4.6
Ni/SrTiO$_3$/MgAl$_2$O$_4$	67	33	3.7
Ni/BaTiO$_3$/MgAl$_2$O$_4$	59	39	4.1

The perovskite-containing samples that are listed in Table 1 were analyzed by Scanning Transmission Electron Microscopy/Energy Dispersive X-ray Spectroscopy (STEM/EDS) and XRD. In all cases, the samples were pretreated while using five redox cycles at 1073 K before the measurements were performed. The results are shown after oxidation at 1073 K and after reduction at 1073 K. Figures 1–3 show the STEM/EDS results for the oxidized and reduced samples. For the oxidized

samples, the images for each of the three samples were indistinguishable from that of the $MgAl_2O_4$ support; and, the EDS maps showed a spatial distribution of A-site cations, Ti, and Ni that matched well with the Mg and Al variations. All of this implies that each of the species deposited by ALD are uniformly distributed over the surface of the $MgAl_2O_4$ support and remain uniformly distributed, even after redox cycling. The $CaTiO_3$, $SrTiO_3$, and $BaTiO_3$ films remained largely unchanged after reduction at 1073 K, but Ni particles were formed on each of the three samples after this treatment. The Ni particles appeared to be slightly smaller for $Ni/CaTiO_3/MgAl_2O_4$, ~10 to 20 nm, and largest on $Ni/BaTiO_3/MgAl_2O_4$, ~30 to 50 nm, with $Ni/SrTiO_3/MgAl_2O_4$ in between. It is noteworthy that the formation of Ni particles was reversible on each of the samples, since the uniform Ni films were restored by oxidation.

Figure 4 reports the XRD patterns for the oxidized and reduced samples. For oxidized $Ni/CaTiO_3/MgAl_2O_4$ and $Ni/SrTiO_3/MgAl_2O_4$, all of the peaks can be assigned to either the $MgAl_2O_4$ support or the corresponding perovskite phase. Upon reduction, peaks that are associated with metallic Ni were also observed. For $BaTiO_3/MgAl_2O_4$, there is significant overlap in the peak positions for $BaTiO_3$ and $MgAl_2O_4$; however, the relative ratio of peaks, particularly those that are centered at 32 and 37 degrees 2θ, make it clear that the major peaks are due to a mixture of $MgAl_2O_4$ and $BaTiO_3$. Small peaks that could be indexed to $BaCO_3$ were also observed on the $Ni/BaTiO_3/MgAl_2O_4$ sample. Again, the XRD pattern of the reduced sample was unchanged, except for the additional features that are associated with metallic Ni.
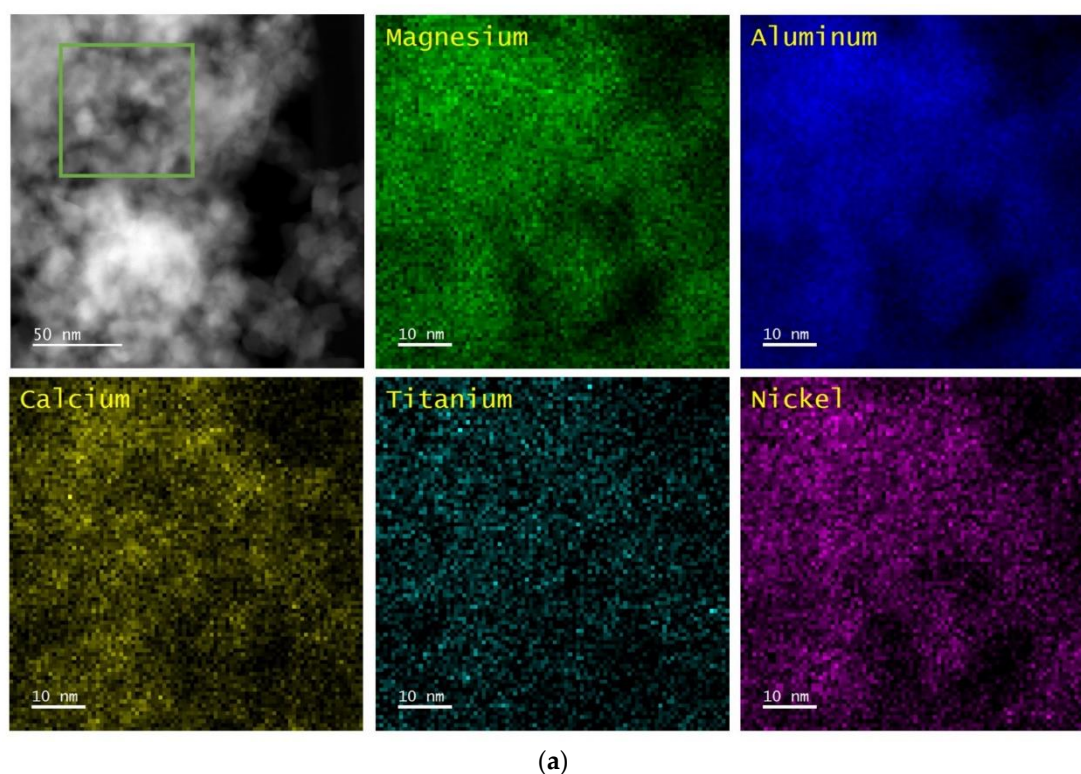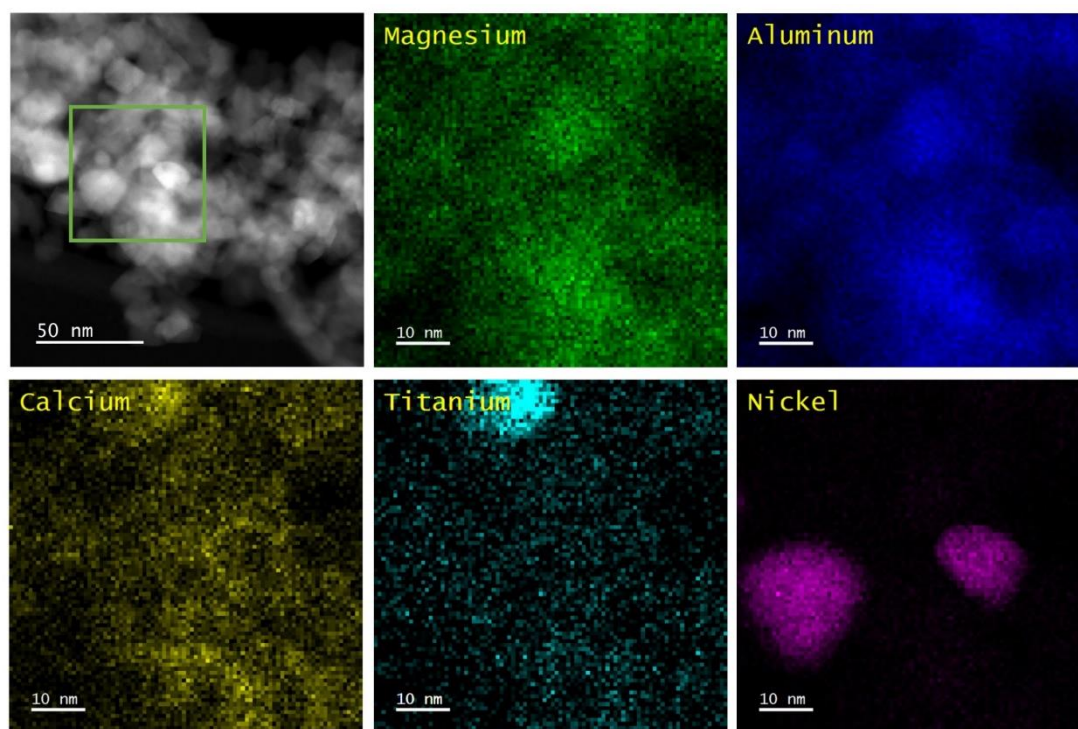

(**a**)

Figure 1. *Cont.*

(**b**)

Figure 1. (**a**) Representative Scanning Transmission Electron Microscopy (STEM) results for Ni/CaTiO$_3$/MgAl$_2$O$_4$ after 1073 K oxidation followed by 773 K reduction with Energy Dispersive X-ray Spectroscopy (EDS) maps of corresponding elements. (**b**) Representative STEM results for Ni/CaTiO$_3$/MgAl$_2$O$_4$ after 1073 K oxidation followed by 1073 K reduction with EDS maps of corresponding elements.
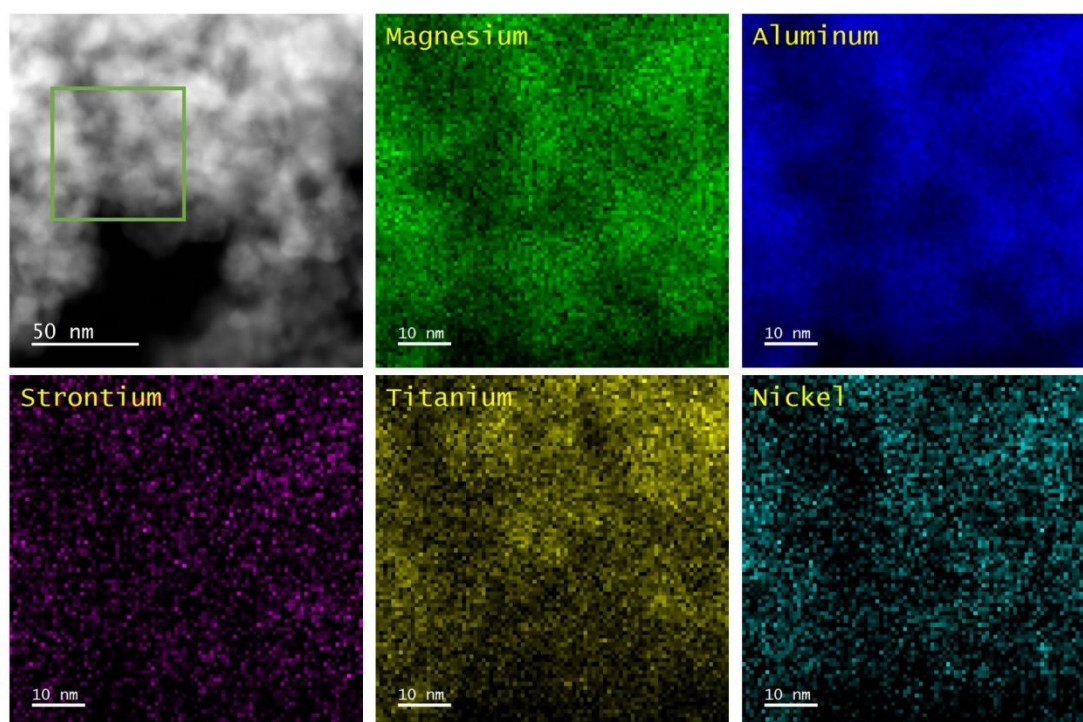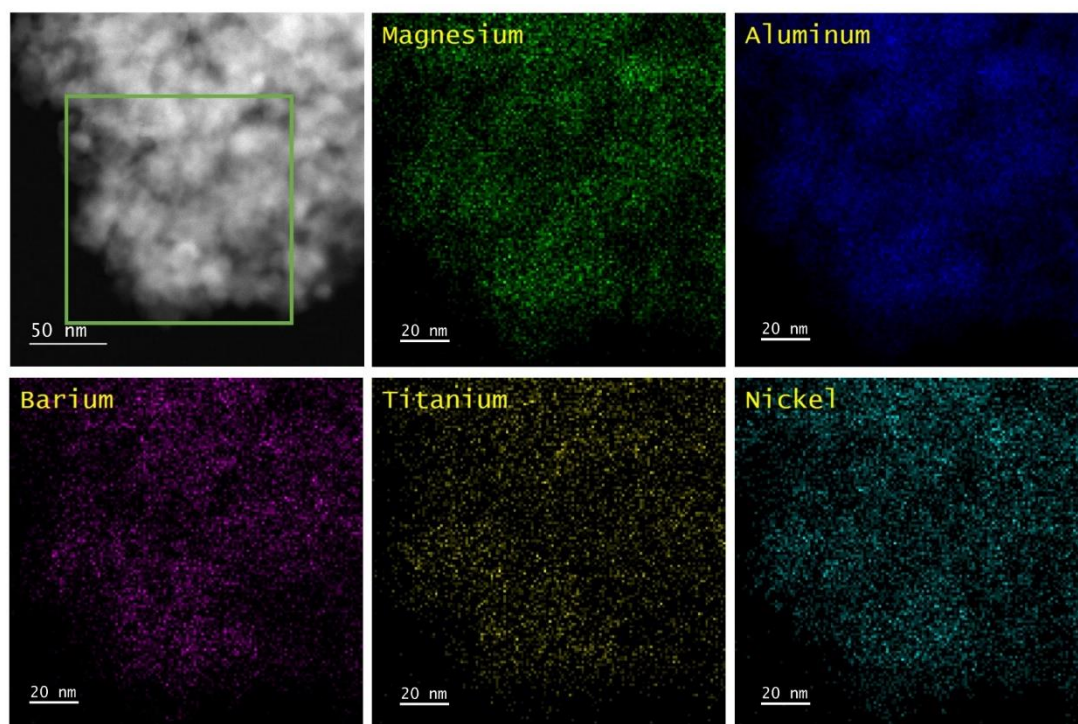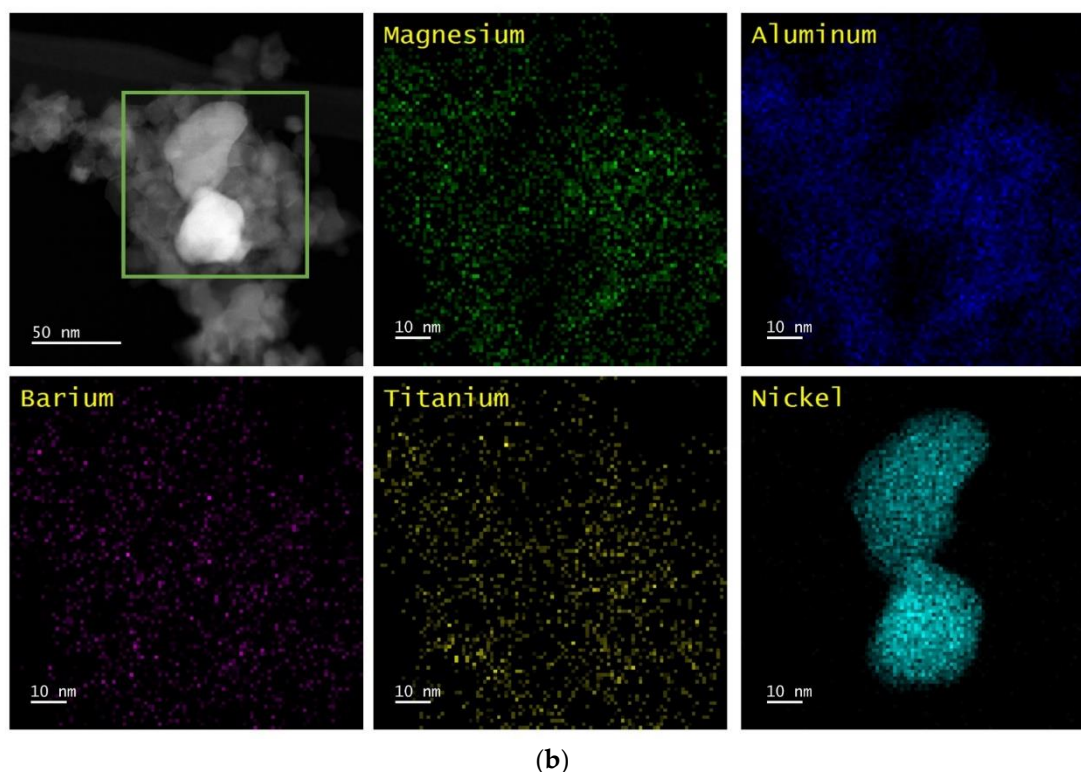

(**a**)

Figure 2. *Cont.*
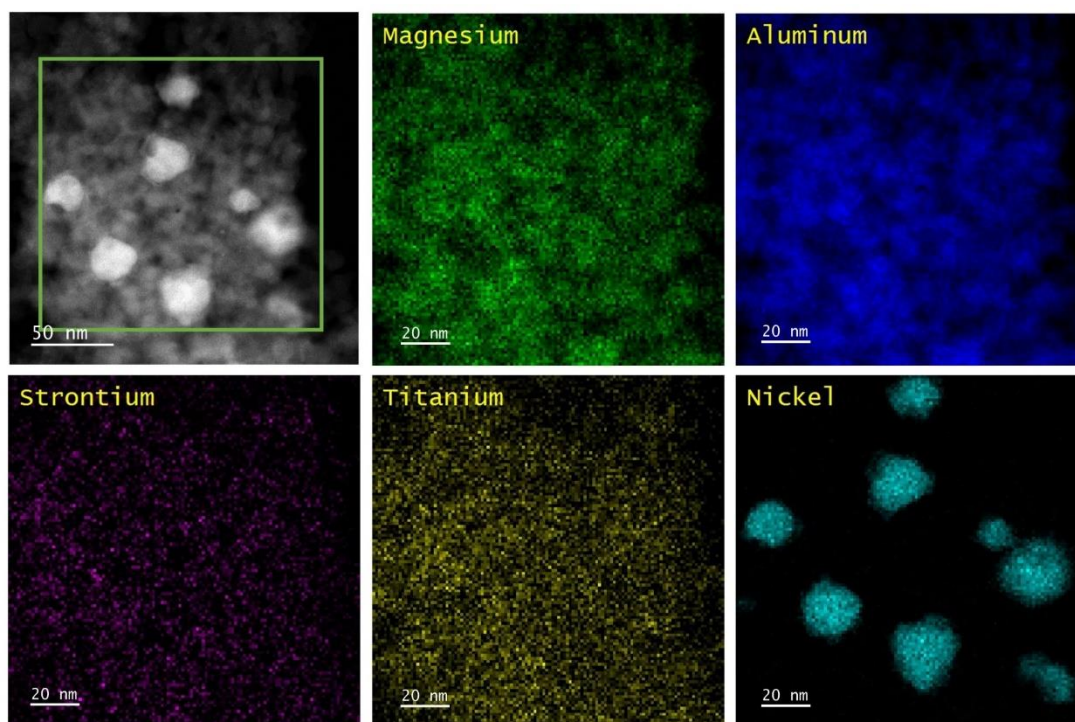
(**b**)

Figure 2. (**a**) Representative STEM results for Ni/SrTiO₃/MgAl₂O₄ after 1073 K oxidation followed by 773 K reduction with EDS maps of corresponding elements. (**b**) Representative STEM results for Ni/SrTiO₃/MgAl₂O₄ after 1073 K oxidation followed by 1073 K reduction with EDS maps of corresponding elements.

(**a**)

Figure 3. *Cont.*

(**b**)

Figure 3. (**a**) Representative STEM results for Ni/BaTiO$_3$/MgAl$_2$O$_4$ after 1073 K oxidation followed by 773 K reduction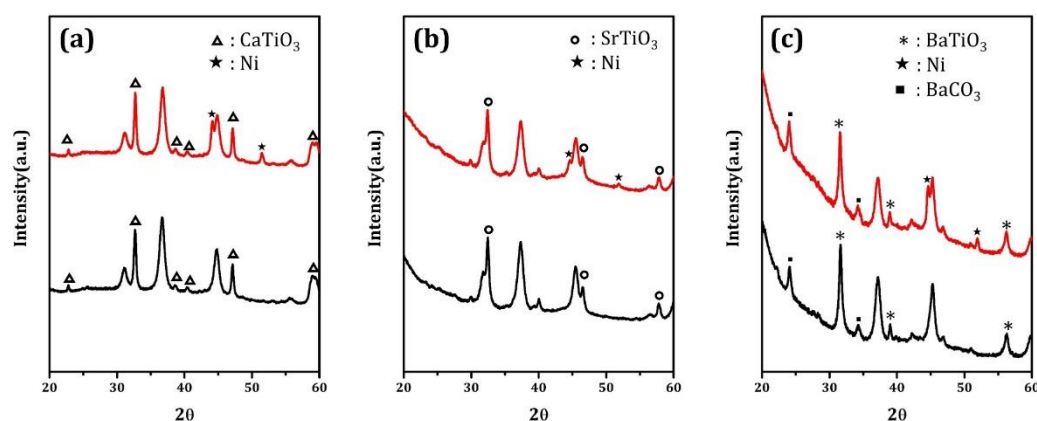 with EDS maps of corresponding elements. (**b**) Representative STEM results for Ni/BaTiO$_3$/MgAl$_2$O$_4$ after 1073 K oxidation, followed by 1073 K reduction with EDS maps of corresponding elements.

Figure 4. X-ray diffraction (XRD) patterns for (**a**) Ni/CaTiO$_3$/MgAl$_2$O$_4$, (**b**) Ni/SrTiO$_3$/MgAl$_2$O$_4$, (**c**) Ni/BaTiO$_3$/MgAl$_2$O$_4$ after (black) 1073 K oxidation followed by 773 K reduction and (red) 1073 K oxidation followed by 1073 K reduction.

As discussed elsewhere [16], the presence of intense perovskite diffraction peaks for uniformly-deposited films that are nominally 1-nm thick suggests the formation of relatively large, two-dimensional crystals, randomly oriented with respect to the support. Based on the width of the peaks, the nominal sizes of the perovskite crystallites are 22 nm for CaTiO$_3$, 18 nm for SrTiO$_3$, and 18 nm for BaTiO$_3$. The particle sizes were also estimated from XRD peak widths for the Ni particles in the reduced samples. These gave reasonable agreement with the values that were obtained from STEM, with values of 21 nm for Ni/CaTiO$_3$/MgAl$_2$O$_4$, 25 nm for Ni/SrTiO$_3$/MgAl$_2$O$_4$, and 31 nm for Ni/BaTiO$_3$/MgAl$_2$O$_4$.

The extent of reduction was measured as a function of temperature for each of the samples in Table 1, with results being shown in Table 2. The samples were first oxidized at 1073 K in flowing air and then reduced in 10%H_2-He mixture at the indicated temperature for 30 min. The amount of oxygen required to completely oxidize the sample at 1073 K was then measured using flow titration. First, there was no measurable reduction of the $CaTiO_3/MgAl_2O_4$ and $SrTiO_3/MgAl_2O_4$ supports, even at 1073 K; but, there was some reduction of the $BaTiO_3/MgAl_2O_4$ sample at the highest temperature. Therefore, with the exception of Ni/$BaTiO_3/MgAl_2O_4$ at 1073 K, the results that are presented in Table 2 indicate the extent of reduction of the Ni in each of the samples. For Ni/$MgAl_2O_4$, only 38% of the Ni was reduced at 773 K and 87% at 1073 K. That such harsh conditions are required for reducing some of the Ni may indicate that a fraction of Ni has reacted with the $MgAl_2O_4$ support after the five redox cycles at 1073 K, with Ni replacing Mg and forming $NiAl_2O_4$. For Ni/$CaTiO_3/MgAl_2O_4$ and Ni/$SrTiO_3/MgAl_2O_4$, a reduction of Ni was insignificant at temperatures below 1073 K. At that temperature, most of the Ni in these samples was reduced. There was some reduction of Ni at lower temperatures on Ni/$BaTiO_3/MgAl_2O_4$, but 1073 K was again required for a majority of the Ni to be reduced.

Table 2. Oxygen uptakes from flow titration for various samples after different reduction pretreatments.

Samples	Oxygen Uptakes (μmol O/g) and Corresponding Ni Reduction Extents * (%) after Dry H_2 Reduction at Various Temperatures			
	773-K Reduction	873-K Reduction	973-K Reduction	1073-K Reduction
Ni/$MgAl_2O_4$	310 (38%)	410 (50%)	490 (59%)	720 (87%)
Ni/$CaTiO_3/MgAl_2O_4$	0 (0%)	0 (0%)	30 (4%)	920 (116%)
Ni/$SrTiO_3/MgAl_2O_4$	0 (0%)	0 (0%)	90 (14%)	700 (109%)
Ni/$BaTiO_3/MgAl_2O_4$	60 (9%)	100 (14%)	230 (33%)	1100 (158%)
$CaTiO_3/MgAl_2O_4$	-	-	-	0
$SrTiO_3/MgAl_2O_4$	-	-	-	0
$BaTiO_3/MgAl_2O_4$	-	-	-	230

* Values in parenthesis indicate % reduction of Ni, assuming oxygen uptake is only for Ni.

Coulometric Titration (CT) measurements were performed at 1073 K on each of the samples in order to better understand the effect of the perovskite supports on Ni reducibility, and the results are shown in Figure 5. At this temperature, tabulated values of ΔG for bulk Ni would indicate that the equilibrium P_{O_2} should be 10^{-14} atm. Data for Ni/$MgAl_2O_4$, reproduced here from a previous publication [20], found that the amount of oxygen that was taken up by the sample was very close to the value obtained from the flow titration reported in Table 2 and that oxidation of the Ni component occurred between 10^{-15} and 10^{-16} atm. The relatively small change in the equilibrium P_{O_2} from that reported for bulk Ni may be due to the Ni particle size or to interactions with the $MgAl_2O_4$ support. The equilibrium P_{O_2} for each of the perovskite-containing samples were shifted to lower values. The shift was the largest for Ni/$CaTiO_3/MgAl_2O_4$, with oxidation occurring in the range of 10^{-18} to 10^{-19} atm, and the smallest for Ni/$BaTiO_3/MgAl_2O_4$, between 10^{-16} and 10^{-17} atm. The Ni/$BaTiO_3/MgAl_2O_4$ sample also took up slightly more oxygen in the CT experiments, which was in agreement with the flow-titration results. Even though the equilibrium P_{O_2} for Ni were shifted to lower values by interactions with the titanates, the changes were less than that previously observed with Ni/$LaFeO_3/MgAl_2O_4$ [20], for which the equilibrium P_{O_2} was 10^{-20} atm at 1073 K.

In order to determine whether these equilibrium properties affect catalytic activities, methane dry reforming (MDR) was investigated in all four Ni catalysts presented in Table 1. In order to determine the effect of reduction temperature on each of the catalysts, methane conversions were measured at 873 K, while using 4.2% CH_4, 8.3% CO_2, and a 72,000 mL·g^{-1}·h^{-1} Gas Hourly Space Velocity (GHSV), and the results are shown in Figure 6a. In each case, the catalysts were oxidized at 1073 K and then

reduced in dry 10% H_2 for 30 min at the indicated temperatures before measuring the conversion. $Ni/MgAl_2O_4$ showed significant conversion after reduction at 773 K, and the conversions increased with the reduction temperature. This corresponds well to the flow-titration results, which indicated that Ni was somewhat reduced on this sample at 773 K, but that higher reduction temperatures increased the fraction of Ni reduction. Each of the perovskite-containing samples was completely inactive for reduction at temperatures below 1073 K, but showed reasonable activity after reduction at that temperature. The differential reaction rates are shown for each of the samples in the Arrhenius plots presented in Figure 6b. The rates were about a factor of two lower on the perovskite-containing samples, but all of the catalysts showed a similar temperature dependence.
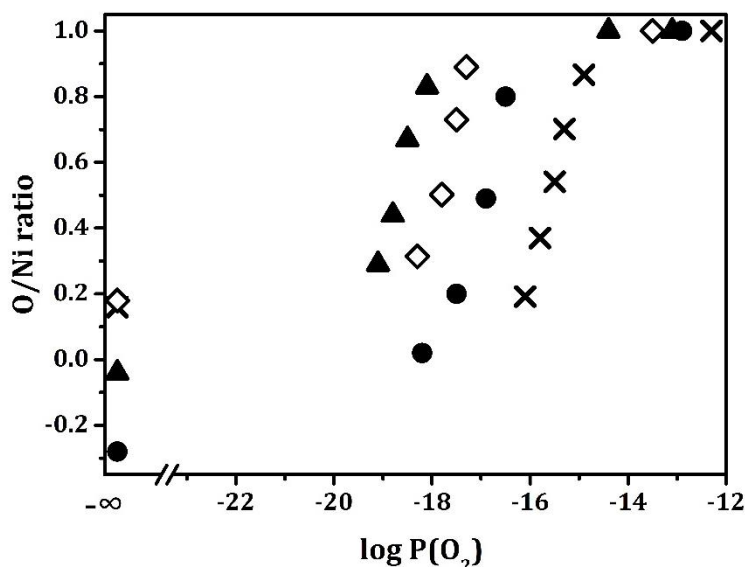
Figure 5. Oxidation isotherm obtained using coulometric titration at 1073 K for (×) $Ni/MgAl_2O_4$; (▲) $Ni/CaTiO_3/MgAl_2O_4$; (◊) $Ni/SrTiO_3/MgAl_2O_4$; and, (•) $Ni/BaTiO_3/MgAl_2O_4$.
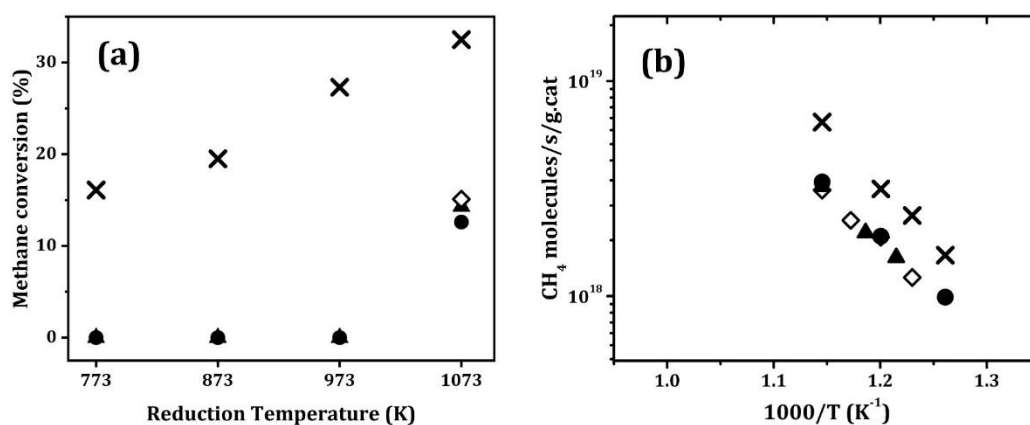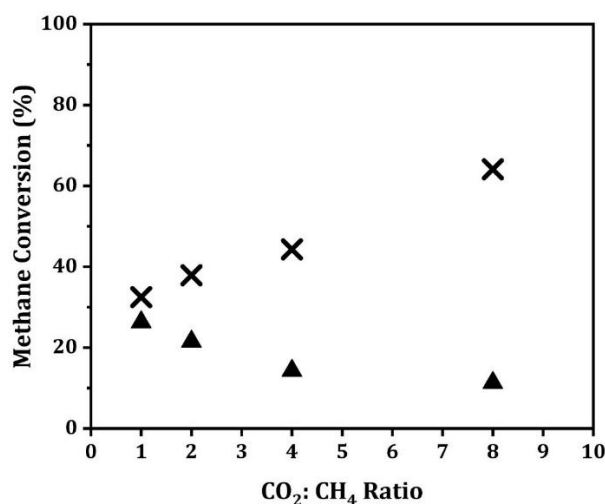

Figure 6. (**a**) Methane conversion for methane dry reforming (MDR) reaction at 873 K as a function of reduction temperature for (×) $Ni/MgAl_2O_4$; (▲) $Ni/CaTiO_3/MgAl_2O_4$; (◊) $Ni/SrTiO_3/MgAl_2O_4$; and, (•) $Ni/BaTiO_3/MgAl_2O_4$. Total flow rate was controlled at 120 mL min^{-1} with CH_4 and CO_2 flow being 5 mL min^{-1} and 10 mL min^{-1}, respectively. (**b**) Arrhenius plots for methane dry reforming (MDR) reaction for (×) $Ni/MgAl_2O_4$; (▲) $Ni/CaTiO_3/MgAl_2O_4$; (◊) $Ni/SrTiO_3/MgAl_2O_4$; and, (•) $Ni/BaTiO_3/MgAl_2O_4$ after each catalyst was reduced at 1073 K. The total flow rate was controlled at 120 mL/min with CH_4 and CO_2 flow being 5 mL min^{-1} and 10 mL min^{-1}, respectively.

With Ni on $LaFeO_3$ films, the shift to lower P_{O_2} in the equilibrium constants for Ni oxidation is sufficient for Ni to be oxidized under some MDR reaction conditions [20]. Although equilibrium

constants for the titanates are significantly closer to that of bulk Ni, we investigated the MDR reaction on $Ni/MgAl_2O_4$ and $Ni/CaTiO_3/MgAl_2O_4$ as a function of the $CH_4:CO_2$ ratio to see whether oxidation of Ni could also occur in these catalysts. The reaction was studied at integral conversions to produce CO and H_2; an equilibrium P_{O_2} is then established by the $CO_2:CO$ ratio. For these measurements, the CH_4 flow rate was kept at 5 mL min^{-1} and the CO_2 and He flows were tuned in order to achieve a desired $CO_2:CH_4$ ratio while keeping the space velocity the same. All of the conversions were measured at 873 K, and the results are shown in Figure 7.

Figure 7. Methane conversion for MDR reaction at 873K for (×) $Ni/MgAl_2O_4$ and (▲) $Ni/CaTiO_3/MgAl_2O_4$ as a function of $CO_2:CH_4$ ratio. The total flow rate and the methane flow rate were controlled at 120 mL/min and 5 mL/min, respectively, while He and CO_2 flows were adjusted accordingly to achieve the desired ratios. The loading is 100 mg for $Ni/MgAl_2O_4$ and 200 mg for $Ni/CaTiO_3/MgAl_2O_4$ in order to ensure similar starting point for the methane conversion. Both of the samples were reduced at 1073K prior to catalytic measurements.

For the $Ni/MgAl_2O_4$ sample, we observed an increase in CH_4 conversion with increasing CO_2 concentration. This is the expected result for reactions with a positive reaction order. For $Ni/CaTiO_3/MgAl_2O_4$, the CH_4 conversion decreased with increasing CO_2 concentration, similar to what was previously observed for $Ni/LaFeO_3/MgAl_2O_4$ [20]. This deactivation was not due to coking, since the conversions shown in Figure 7 were stable and did not depend on whether the CO_2 concentration was increasing or decreasing. With the $LaFeO_3$-supported Ni, the deactivation was easier to observe because of the larger change in the equilibrium constant.

3. Discussion

Much of the work on perovskite-supported catalysts has focused on their exsolution properties and resistance to sintering. Thin-film perovskite supports are not identical to bulk perovskites, since the films are thinner than the nominal particle size of the metals, as discussed in more detail elsewhere [16]. However, there are many similarities between the bulk and thin-film supports, which suggests that bonding interactions at the metal-perovskite interface are similar in these two cases.

In agreement with a previous study of Ni on $LaFeO_3$ films [20], the work presented here demonstrates that the support can affect the oxidation thermodynamics of the Ni. Because the electronic effects of the support on a metal can only extend to a few atomic distances from the interface [21], most of the Ni must be in direct contact with the support. Indeed, the STEM/EDS data indicate that is the case, at least for the oxidized samples. While thermodynamic properties do not indicate how large the kinetic barriers will be for reduction, the fact that the perovskite-supported catalysts require high temperatures for Ni reduction is additional evidence that there must be strong bonding interactions between the support and Ni.

Changes in Ni geometry upon different pretreatments are also worth noting. While previous studies suggested that interactions between Ni and some supports can lead to the redispersion of Ni, the conditions used were found to be harsher and the redispersion less complete than the results that are reported here [22]. Our results would indicate that Ni atoms can migrate relatively long distances, along the surface of the perovskite thin films. It seems likely that Ni is incorporated as a strongly interacting phase, different from normal NiO, when supported on perovskite thin films, thus leading to the changes in equilibrium P_{O_2}.

Similar to what we observed in an earlier study of Rh on $CaTiO_3$, $SrTiO_3$, and $BaTiO_3$ films, support interactions depend on the A-site cations in this series. With Rh, the differences were much stronger than what we observed here with Ni. Rh that was supported on $CaTiO_3/MgAl_2O_4$ was almost unreducible and catalytically inactive, while the support effects for Rh on $BaTiO_3/MgAl_2O_4$ were negligible. The ordering of support interactions for Ni were the same as with Rh, in that $CaTiO_3$ interacts most strongly and $BaTiO_3$ least. How the A-site cations affect these interactions is uncertain. One possibility is that differences in the surface energies of these titanates change the surface terminations. For example, we have previously established by Low Energy Ion Scattering that $CaTiO_3$ films are terminated by Ca [18] and it is possible that $BaTiO_3$ prefers to be B-site terminated due to the relative sizes of the ions. The free volumes for these three perovskite materials also change with the size of the A-site cations, and this may affect how easily catalytic metal cations can enter the lattice.

It is also interesting to ask why the differences for Ni on the various titanates were less than what was observed for Rh. One possible reason for this could be the nominal charge on the cations. It was previously shown that Pd, which, like Ni, is expected to exist in the +2 state when oxidized, does not interact with $CaTiO_3$ and it cannot enter the $CaTiO_3$ lattice [18]. The ability of Rh to have multiple, stable oxidation states may also play a role in allowing Rh to interact more strongly with the perovskite lattices.

There is obviously much that we still need to learn about both ex-solution catalysts and the differences between bulk and thin-film perovskites. The fact that support interactions with these perovskite-supported metals are so specific to the compositions of the metal and the support represents both a challenge and an opportunity to tailor the catalytic properties for specific applications.

4. Materials and Methods

$MgAl_2O_4$ was prepared in our laboratory and had a surface area of 120 m^2/g after being stabilized by calcination to 1173 K, as described elsewhere [17,23]. The equipment and procedures used for ALD have also been reported previously [24,25]. The system is essentially a high-temperature adsorption apparatus that is attached to a mechanical vacuum pump. The evacuated samples were exposed to vapors from the precursors for approximately 10 min before purging excess precursor by evacuation. The precursors choices for the A-site cations were the same as one of the previous publications [17], bis(2,2,6,6-tetramethyl-3,5-heptanedionato) calcium (Ca(TMHD)$_2$, Strem, Newburyport, MA, USA), bis(2,2,6,6-tetramethyl-3,5-heptanedionato) strontium hydrate (Sr(TMHD)$_2$, Strem, USA), and bis(2,2,6,6-tetramethyl-3,5-heptanedionato) barium hydrate (Ba(TMHD)$_2$, Strem, USA) were chosen for Ca, Sr, and Ba ALD processes, respectively, and the exposure was carried out at 573 K. Because the TMHD ligands can only be removed at elevated temperatures by air [26], the oxidation step of the ALD cycle for these precursors was performed by transferring the samples to a muffle furnace at 773 K for 5 min. For the TiO_2-ALD process, Titanium chloride ($TiCl_4$, Sigma-Aldrich, St. Louis, MO, USA) was chosen as the precursor. $TiCl_4$ was kept at 363 K to ensure the generation of a sufficient amount of the precursor vapor. The deposition and the oxidation were both performed at 423 K. For the deposition half cycle, the samples were exposed to $TiCl_4$ vapor for three times for 1 min. After that, humidified air (10% water content) was introduced to the sample to ensure complete oxidation. Ni was also deposited by ALD while using Ni(TMHD)$_2$ (Strem, USA) as the precursor and a deposition temperature of 523 K.

The ALD growth rates were measured gravimetrically and checked by Inductively Coupled Plasma Optical Emission Spectrometry (ICP-OES, Spectro Genesis). The dissolution processes were performed at 333 K overnight while using 10 mL of *aqua regia* for the samples. After that, the solutions were diluted to suitable ranges for ICP measurements. The X-ray diffraction (XRD) patterns were recorded on a Rigaku MiniFlex diffractometer that was equipped with a Cu Kα source (λ = 0.15416 nm) and then patterns for 2 theta range from 20 to 60 degrees were recorded. BET surface areas were measured while using homebuilt equipment at 78 K [24]. *Ex-situ* Scanning Transmission Electron Microscopy and Energy Dispersive X-ray Spectroscopy (STEM-EDS) measurements were performed using a JEOL NEOARM operated at 200 kV.

The rates for methane dry reforming were determined from differential conversions in a 0.25-inch, quartz, tubular-flow reactor at atmospheric pressure, with products analyzed while using a gas chromatograph (SRI 8610C) that was equipped with a TCD detector. The catalyst loadings were 100 mg for all of the samples. The total gas flow rate was maintained at 120 mL min^{-1}. Methane flow was kept at 5 mL min^{-1} throughout the measurements. CO_2 and He flows were adjusted to achieve different CO_2:CH_4 ratios while maintaining a constant flow rate.

The reducibilities of the samples were quantified by flow titration and Coulometric Titration (CT), as described in detail elsewhere [25]. The flow-titration experiments were performed in a tubular reactor at 1 atm with 200-mg samples. After reducing the samples in flowing H_2 at desired temperatures, followed by purging with He, the samples were exposed to dry air at 1073 K at a flow rate of 5 mL min^{-1} while monitoring the reactor effluent with a mass spectrometer. The O_2 uptake was then determined by integrating the difference between the N_2 and O_2 signals in the effluent. Equilibrium constants for oxidation of Ni were probed by CT at 1073 K. In a CT experiment, 500-mg samples were placed in the center of a YSZ (Yttria-Stabilized Zirconia) tube that had Pt paste on the inner wall and Ag paste on the outer wall. After flowing a mixture of 10% H_2, 10% H_2O, and 80% He over the sample at 1073 K, the tube was sealed with cajon fittings. The known quantities of oxygen were then electrochemically pumped into or out of the YSZ tube by applying a known charge across the metal electrodes using a Gamry instruments potentiostat. The equilibrium P_{O_2} was calculated from the electrode open-circuit potential while using the Nernst Equation after allowing the system to come to equilibrium with the electrodes at open circuit.

5. Conclusions

Ni catalysts that were supported on 1 nm films of $CaTiO_3$, $SrTiO_3$, and $BaTiO_3$ on $MgAl_2O_4$ were found to have different properties as compared to the Ni/$MgAl_2O_4$ catalyst. 1073-K reduction is required to activate the Ni/$ATiO_3$/$MgAl_2O_4$ catalysts. By contrast, the Ni/$MgAl_2O_4$ catalyst was found to be active for methane dry reforming (MDR) upon 773-K reduction, and the catalytic performance increased with reduction temperature due to a more complete reduction of Ni. Equilibrium oxidation constants for Ni, which were obtained from Coulometric Titration (CT), suggested that the equilibrium PO_2 for Ni oxidation is shifted to lower values for the Ni/$ATiO_3$/$MgAl_2O_4$ samples. The equilibrium PO_2 for Ni oxidation was found to decrease in the order of Ni/$CaTiO_3$/$MgAl_2O_4$ < Ni/$SrTiO_3$/$MgAl_2O_4$ < Ni/$BaTiO_3$/$MgAl_2O_4$ < Ni/$MgAl_2O_4$. Consequently, catalyst deactivation was observed on the Ni/$CaTiO_3$/$MgAl_2O_4$ sample when increasing the feed CO_2:CH_4 ratio, which was potentially due to Ni oxidation or changes in Ni reaction order.

Conflicts of Interest: The authors declare no conflict of interest.

References

1. Tanaka, H.; Taniguchi, M.; Uenishi, M.; Kajita, N.; Tan, I.; Nishihata, Y.; Mizuki, J.I.; Narita, K.; Kimura, M.; Kaneko, K. Self-regenerating Rh-and Pt-based perovskite catalysts for automotive-emissions control. *Angew. Chem. Int. Ed.* **2006**, *45*, 5998–6002. [CrossRef] [PubMed]

2. Nishihata, Y.; Mizuki, J.; Akao, T.; Tanaka, H.; Uenishi, M.; Kimura, M.; Okamoto, T.; Hamada, N. Self-regeneration of a Pd-perovskite catalyst for automotive emissions control. *Nature* **2002**, *418*, 164. [CrossRef] [PubMed]

3. Tanaka, H.; Tan, I.; Uenishi, M.; Kimura, M.; Dohmae, K. Regeneration of palladium subsequent to solid solution and segregation in a perovskite catalyst: An intelligent catalyst. *Top. Catal.* **2001**, *16*, 63–70. [CrossRef]

4. Uenishi, M.; Taniguchi, M.; Tanaka, H.; Kimura, M.; Nishihata, Y.; Mizuki, J.; Kobayashi, T. Redox behavior of palladium at start-up in the Perovskite-type LaFePdO$_x$ automotive catalysts showing a self-regenerative function. *Appl. Catal. B Environ.* **2005**, *57*, 267–273. [CrossRef]

5. Tanaka, H.; Fujikawa, H. Perovskite-Pd three-way catalysts for automotive applications. In *SAE Technical Paper*; SAE International: Warrendale, PA, USA, 1993.

6. Tanaka, H.; Uenishi, M.; Taniguchi, M.; Tan, I.; Narita, K.; Kimura, M.; Kaneko, K.; Nishihata, Y.; Mizuki, J.i. The intelligent catalyst having the self-regenerative function of Pd, Rh and Pt for automotive emissions control. *Catal. Today* **2006**, *117*, 321–328. [CrossRef]

7. Tanaka, H.; Fujikawa, H.; Takahashi, I. Excellent oxygen storage capacity of perovskite-Pd three-way catalysts. *Sae Trans.* **1995**, 289–301.

8. Tanaka, H.; Taniguchi, M.; Kajita, N.; Uenishi, M.; Tan, I.; Sato, N.; Narita, K.; Kimura, M. Design of the intelligent catalyst for Japan ULEV standard. *Top. Catal.* **2004**, *30*, 389–396. [CrossRef]

9. Marcucci, A.; Zurlo, F.; Sora, I.N.; Placidi, E.; Casciardi, S.; Licoccia, S.; Di Bartolomeo, E. A redox stable Pd-doped perovskite for SOFC applications. *J. Mater. Chem. A* **2019**, *7*, 5344–5352. [CrossRef]

10. Zhu, T.; Troiani, H.E.; Mogni, L.V.; Han, M.; Barnett, S.A. Ni-substituted Sr(Ti, Fe)O$_3$ SOFC anodes: Achieving high performance via metal alloy nanoparticle exsolution. *Joule* **2018**, *2*, 478–496. [CrossRef]

11. Oemar, U.; Ang, M.; Hee, W.; Hidajat, K.; Kawi, S. Perovskite La$_x$M$_{1-x}$Ni$_{0.8}$Fe$_{0.2}$O$_3$ catalyst for steam reforming of toluene: Crucial role of alkaline earth metal at low steam condition. *Appl. Catal. B Environ.* **2014**, *148*, 231–242. [CrossRef]

12. Deng, J.; Cai, M.; Sun, W.; Liao, X.; Chu, W.; Zhao, X.S. Oxidative Methane Reforming with an Intelligent Catalyst: Sintering-Tolerant Supported Nickel Nanoparticles. *ChemSusChem* **2013**, *6*, 2061–2065. [CrossRef] [PubMed]

13. Chai, Y.; Fu, Y.; Feng, H.; Kong, W.; Yuan, C.; Pan, B.; Zhang, J.; Sun, Y. A Nickel-Based Perovskite Catalyst with a Bimodal Size Distribution of Nickel Particles for Dry Reforming of Methane. *ChemCatChem* **2018**, *10*, 2078–2086. [CrossRef]

14. Neagu, D.; Oh, T.-S.; Miller, D.N.; Ménard, H.; Bukhari, S.M.; Gamble, S.R.; Gorte, R.J.; Vohs, J.M.; Irvine, J.T. Nano-socketed nickel particles with enhanced coking resistance grown in situ by redox exsolution. *Nat. Commun.* **2015**, *6*, 1–8. [CrossRef] [PubMed]

15. Oh, T.-S.; Rahani, E.K.; Neagu, D.; Irvine, J.T.; Shenoy, V.B.; Gorte, R.J.; Vohs, J.M. Evidence and model for strain-driven release of metal nanocatalysts from perovskites during exsolution. *J. Phys. Chem. Lett.* **2015**, *6*, 5106–5110. [CrossRef] [PubMed]

16. Mao, X.; Lin, C.; Graham, G.W.; Gorte, R.J. A Perspective on Thin-Film Perovskites as Supports for Metal Catalysts. *ACS Catal.* **2020**, *10*, 8840–8849. [CrossRef]

17. Lin, C.; Foucher, A.C.; Ji, Y.; Stach, E.A.; Gorte, R.J. Investigation of Rh–Titanate (ATiO$_3$) Interactions on High-Surface-Area Perovskite Thin Films Prepared by Atomic Layer Deposition. *J. Mater. Chem. A* **2020**, *8*, 16973–16984. [CrossRef]

18. Lin, C.; Foucher, A.C.; Ji, Y.; Curran, C.D.; Stach, E.A.; McIntosh, S.; Gorte, R.J. "Intelligent" Pt catalysts studied on high-surface-area CaTiO$_3$ films. *ACS Catal.* **2019**, *9*, 7318–7327. [CrossRef]

19. Lin, C.; Jang, J.B.; Zhang, L.; Stach, E.A.; Gorte, R.J. Improved Coking Resistance of "Intelligent" Ni Catalysts Prepared by Atomic Layer Deposition. *ACS Catal.* **2018**, *8*, 7679–7687. [CrossRef]

20. Mao, X.; Foucher, A.C.; Stach, E.A.; Gorte, R.J. Changes in Ni-NiO equilibrium due to LaFeO$_3$ and the effect on dry reforming of CH$_4$. *J. Catal.* **2020**, *381*, 561–569. [CrossRef]

21. Ro, I.; Resasco, J.; Christopher, P. Approaches for understanding and controlling interfacial effects in oxide-supported metal catalysts. *ACS Catal.* **2018**, *8*, 7368–7387. [CrossRef]

22. Remiro, A.; Arandia, A.; Oar-Arteta, L.; Bilbao, J.; Gayubo, A.G. Regeneration of NiAl$_2$O$_4$ spinel type catalysts used in the reforming of raw bio-oil. *Appl. Catal. B Environ.* **2018**, *237*, 353–365. [CrossRef]

23. Onn, T.M.; Monai, M.; Dai, S.; Fonda, E.; Montini, T.; Pan, X.; Graham, G.W.; Fornasiero, P.; Gorte, R.J. Smart Pd catalyst with improved thermal stability supported on high-surface-area LaFeO$_3$ prepared by atomic layer deposition. *J. Am. Chem. Soc.* **2018**, *140*, 4841–4848. [CrossRef] [PubMed]

24. Onn, T.M.; Zhang, S.; Arroyo-Ramirez, L.; Chung, Y.-C.; Graham, G.W.; Pan, X.; Gorte, R.J. Improved thermal stability and methane-oxidation activity of Pd/Al$_2$O$_3$ catalysts by atomic layer deposition of ZrO$_2$. *ACS Catal.* **2015**, *5*, 5696–5701. [CrossRef]

25. Onn, T.M.; Mao, X.; Lin, C.; Wang, C.; Gorte, R.J. Investigation of the thermodynamic properties of surface ceria and ceria–zirconia solid solution films prepared by atomic layer deposition on Al$_2$O$_3$. *Inorganics* **2017**, *5*, 69.

26. Lin, C.; Mao, X.; Onn, T.M.; Jang, J.; Gorte, R.J. Stabilization of ZrO$_2$ powders via ALD of CeO$_2$ and ZrO$_2$. *Inorganics* **2017**, *5*, 65. [CrossRef]